Macromolecular Research, Vol. 14, No. 6, pp 596-602 (2006)

# Effect of High-Temperature Spinning and PVP Additive on the Properties of PVDF Hollow Fiber Membranes for Microfiltration

**Bong Jun Cha* and Jung Mok Yang**

*Division of Environmental Engineering and Biotechnology, Myongji University, Gyeonggi 449-728, Korea*

*Received May 24, 2006; Revised October 27, 2006*

**Abstract:** The effect of high-temperature spinning and poly(vinyl pyrrolidone) (PVP) additive on poly(vinylidene fluoride) (PVDF) hollow fiber membranes was investigated using differential scanning calorimetry, X-ray diffraction measurement, and scanning electron microscopy, together with the corresponding microfiltration performances such as water flux, rejection rate, and elongational strength. Using high-temperature spinning, porous hollow fiber membranes with particulate morphology were prepared through PVDF crystallization. The particulate structure of the membranes was further modified by the addition of miscible PVP with PVDF. Due to these effects, the rejection rate and strength of the fibers were increased at the expense of reduced water flux and mean pore size, which indicates that high-temperature spinning and PVP addition are very effective to control the morphology of PVDF hollow fiber membranes for microfiltration.

*Keywords*: poly(vinylidene fluoride), poly(vinyl pyrrolidone), high-temperature spinning, hollow membrane, microfiltration.

## Introduction

Recently, semicrystalline poly(vinylidene fluoride) (PVDF) as a membrane forming material has attracted wide attention owing to both its feasibility of membrane formation and good mechanical properties as well as its intrinsic exceptional chemical and thermal stability.[1] The various PVDF membranes including flat sheet and hollow fiber types were produced by the conventional immersion precipitation (IP) method and the size-selective properties accompanied by the morphological changes were thoroughly investigated depending on the preparation conditions such as choice of solvent, concentration, and temperature.[2-4] As well known, the IP process uses liquid-liquid phase separation and/or crystallization triggered by the exchange of solvent for non-solvent phase which resulted in porous structured membranes ranging from nano- to micro-scale pore sizes.[5]

For further structural control of the porous membranes, a variety of additives such as macromolecules, small organic materials, and inorganic salts or particles has also been introduced. Among such additives, the use of poly(vinyl pyrrolidone) (PVP) is gaining much interest because of its non-toxicity, good miscibility with various polymers such as poly(acrylonitrile) (PAN), poly(sulfone) (PSU), and poly (ether imide) (PEI), and the enhancement of hydrophilicity against hydrophobic matrix polymer.[6-10] Moreover, the addition of PVP may significantly change surface properties of microfiltration (MF) and ultrafiltration (UF) membranes as well as their filtration performance and porous structure. For instance, it was reported that the membranes with asymmetric structure without macrovoids was prepared through PVP addition, leading to the enhancement of hydrophilicity.[8] However, this change of surface property was also concomitant with the decrease of water flux by the reduction of apparent pore sizes due to the swelling of PVP entrapped into pore walls.[9] Since it is well known that PVDF is very miscible with PVP, the microporous structure of PVDF membranes has been further modified using PVP for UF applications.[11] Nevertheless, to produce optimized MF membrane with balanced permeation and rejection rate, the porous structures of the membranes should further be controlled under the pore size of 0.1 $\mu$m. Furthermore, systematic studies about the structural control of PVDF hollow fiber membranes using PVP still need to be explored to develop a membrane with the desirable MF performance.

As an alternative to IP, the thermally-induced phase separation (TIPS) process has been introduced to prepare microporous membranes. Due to its intrinsic advantages over IP process, the TIPS process has been applied to a wide range of crystalline polymers and more details of membrane for-

*Corresponding Author. E-mail: bjchans@mju.ac.kr

mation using TIPS process were reported elsewhere.[12-14] The preparation of membrane from TIPS system generally employs a binary mixture consisted of polymer and diluent at very high temperature above melting temperature of polymer. Although this approach is particularly valuable owing to more simplified control parameters than those in IP process, the wide use of TIPS process can be limited by the choice of diluent and high process temperature. Thus, it is believed that the use of solvent with wide solubility at relatively low temperature is quite desirable to take advantage of TIPS process.

In this study, PVDF hollow fiber membranes with different microporous structures were prepared using $\gamma$-butyrolactone ($\gamma$-BL) which is a poor solvent for PVDF and high-temperature spinning similar to the conventional TIPS process. The formed microporous structures were tailored further by the addition of PVP as a structural modifier for optimized MF performance. While most of the porous PVDF membranes have been performed through conventional IP process, the effect of high-temperature spinning method together with PVP addition on PVDF MF performances and structural transition has not been presented in detail, which is the main objective of the present study.

## Experimental

**Materials.** PVDF (Solef 1015, $M_w$; 261,000, density; 1.78 g/cm$^3$) was supplied by Solvay Korea Co. Ltd.. Reagent grades, $\gamma$-butyrolactone ($\gamma$-BL), dimethylacetamide (DMAc), and ethylene glycol (EG) were obtained from Samchun Pure Chemicals. Poly(vinyl pyrrolidone) (PVP) with various molecular weights of 10,000, 55,000 and 900,000 were purchased from Aldrich. All chemicals and materials were used without further purification.

**Preparation of Hollow Fiber Membrane.** PVDF and PVP in powder form were dissolved at 140 °C in $\gamma$-BL, to obtain a clear and homogeneous solution comprising of 36 wt% of PVDF and 3 wt% of PVP. After degasification, the dope solution was transported to a spinning nozzle by a gear pump. The jacket type pump head and nozzle were also maintained at 140 °C and the polymer solution was subsequently spun into the coagulation bath composed of 6/4 weight ratio of EG/DMAc, maintained at 20 °C. The inner coagulant composed of EG/DMAc mixture was also used for all spinning conditions with a fixed air gap of 10 cm. After precipitation into the coagulation bath, the as-spun hollow fiber membranes were rolled to a take-up machine and were further washed for 120 hrs to remove the residual solvent in tap water. For comparison, hollow fiber membranes without PVP were produced under the same preparation conditions. For module preparation, some of the wet fibers were immersed for 24 hrs into a 50 wt% glycerin aqueous solution before drying in ambient conditions. A test module containing 6 fibers with an effective length of 10 cm was made using an acryl tube with a diameter of 10 mm and epoxy as potting material.

**Differential Scanning Calorimetry.** The thermal properties of the samples were obtained with a TA instrument DSC Q10 operated under a nitrogen atmosphere. Membranes were dried in a convection oven at 60 °C for three days. Samples (3-4 mg) were sealed in an aluminum pan, heated from 30 to 300 °C at a rate of 10 °C/min. After maintaining for 10 min, a cooling scan was then performed at a rate of 10 °C/min down to 30 °C. A subsequent heating run was taken after equilibrating the sample at 30 °C for 10 min.

**X-Ray Diffraction Study.** X-ray diffraction experiments were performed on a PANalytical (X'Pert-Pro) multi-purpose diffractometer using Cu$K_\alpha$ radiation ($1.54 \times 10^{-10}$ m) for all hollow fiber samples. A rotating anode generator with a copper target was operated at 40 kV of the acceleration voltage with 30 mA supplied current. All samples were analyzed in continuous scan mode (counting 0.5 s per 0.020° 2$\theta$) from 5 to 60° 2$\theta$. Data was collected using X'Pert Industry and analyzed using Highscore software packages (PANalytical Ltd.).

**Scanning Electron Microscopy.** Scanning electron microscopy (Hitachi model S-3500N) was employed to investigate the outer surface and cross-sectional morphologies of the hollow fiber. The membranes were fractured into small pieces in liquid nitrogen and fixed on a sample holder to analyze the membrane structure. In order to minimize fiber damage due to the electron beam and to obtain clear images, platinum palladium alloy was sputtered onto the fiber samples.

**Determination of Mean Pore Size.** The mean pore size of the membranes were determined using a capillary flow porometer (Porous Materials Inc., model CFP-1200AE), which gives information about the constricted part of the through pore diameters in the 0.033-500 $\mu$m range. The analysis is based upon a three-curve graph: dry curve, wet curve and half-dry curve, as reported previously.[15] To get the dry curve, a dry hollow fiber membrane was placed into the test module containing three fibers, nitrogen gas pressure was increased on the inner side of the sample, and the flow rate and gas pressure were measured. To attain the wet curve, the same membrane was saturated with a wetting fluid with known surface tension (Galwick; 15.9 dyne/cm) and gas pressure was increased on one side of the sample. The mean flow pore diameter was determined from the mean flow pressure wherein the half-dry curve intersected with the wet curve at a differential pressure.

**Water Flux and Rejection Rate.** Pure water flux test was performed with a dead-end type membrane module, which was connected to a thermostatic bath (Millipore Co., 5 L) pressurized with nitrogen gas at 25 °C. Water flux under a feed pressure of 1 kg/cm$^2$ was determined by measuring the volume of permeate that penetrated a specified area of membrane per unit time using deionized water. The solute rejection rate was performed with polystyrene latex particle

(Polyscience, particle diameter; 100 nm) dispersed in deionized water. The concentrations of feed and permeate solution were determined using ultraviolet-visible spectrophotometer (Shimadzu, UV1601-PC) at 240 nm. The rejection rate ($R$) was calculated by $R=1-(C_p/C_f)$, where $C_p$ and $C_f$ are the concentrations of the permeate and feed, respectively.

**Measurement of Elongation Strength.** Using an Instron 4303 Universal Tester (ASTM D 638M) the elongation strength of the fibers was measured using a grip distance of 100 mm and a cross-head speed of 50 mm/min with a load cell of 10 N. All strength values reported here were averaged over three measurements.

**FTIR Measurement.** FTIR measurements were performed on a Varian 2000 FTIR spectrometer in mode of the attenuated total reflectance (ATR-FTIR) using a Ge crystal detector with an incident angle of 45°. For each sample, 16 scans were signal-averaged at a resolution of 4 $cm^{-1}$. Baseline corrected infrared spectra were obtained for all fibers in absorbance mode at room temperature.

## Results and Discussion

**Phase Diagram.** In the typical TIPS process, phase diagram is composed of the binodal line determined by the measurement of cloud points, as reported elsewhere.[12,13] However, for the PVDF/$\gamma$-BL system, it is important to note that the phase diagram was represented by sol-gel transition temperature instead of binodal line since the binodal line or liquid-liquid phase separation line is below sol-gel transition temperature and thereby crystallization of PVDF inhibits the observation of binodal line.[16,17] This was further demonstrated by the fact that PVDF/$\gamma$-BL solutions show the sol-gel transition from a sol state to a physical gel with cooling by the mechanism of crystallization-induced gelation.[16-18] Thus, phase diagram based on the sol-gel transition temperature was determined at varying polymer concentrations using test-tube tilting method. A test-tube tilting method determines whether the status of the solution is a sol (flow) or a gel (no flow). Different concentrations of the homogenous solutions contained in vials were set at a fixed temperature for 12 hrs intervals. Then, the solution is judged to be in the sol state if the level meniscus deformed under its own weight after test-tube tilting. A gelled status is obtained if the meniscus could not be seen to deform, as described previously.[15,16] Thus, above the transition temperature, the solution presents a clear sol state while a turbid gel composed of a number of crystalline particulates appears below temperature. It is noted that the sol-gel transition temperature had an influence on the determination of spinning temperature for hollow fiber preparation, since the spinning of the dope solution on a gelled state practically requires a very precise temperature control to sta-bilize the fiber spinning process. Thus, to avoid gelation, the spinning temperature for membrane formation was chosen at 140 °C with polymer concentration of 36 wt%.[19]

**Morphological Study of PVDF Hollow Fibers.** A dope solution was first spun into the coagulation bath with EG/DMAc mixture of 6/4 (w/w) ratio through a spinneret maintained at 140 °C for high-temperature spinning. Figure 1 shows the surface SEM photographs of PVDF hollow fiber membranes having PVP of various molecular weights as well as the membrane without PVP. It can be seen that the outer surfaces of the all samples were composed of a number of polygonal crystalline domains with particulate morphology and partially dendrite crystalline phases. From the magnified images, it is interesting to detect the presence of some slit-type pores among many dendrite crystallites with pore sizes below 1 $\mu$m. Based on morphological studies, it is well known that liquid-liquid demixing reveals cellular structures composed of sponge- or finger-like morphology that form due to the exchange of solvent with non-solvent. In contrast, crystallization leads to a particulate morphology composed of lamella structures. Hence, this formation of crystalline units

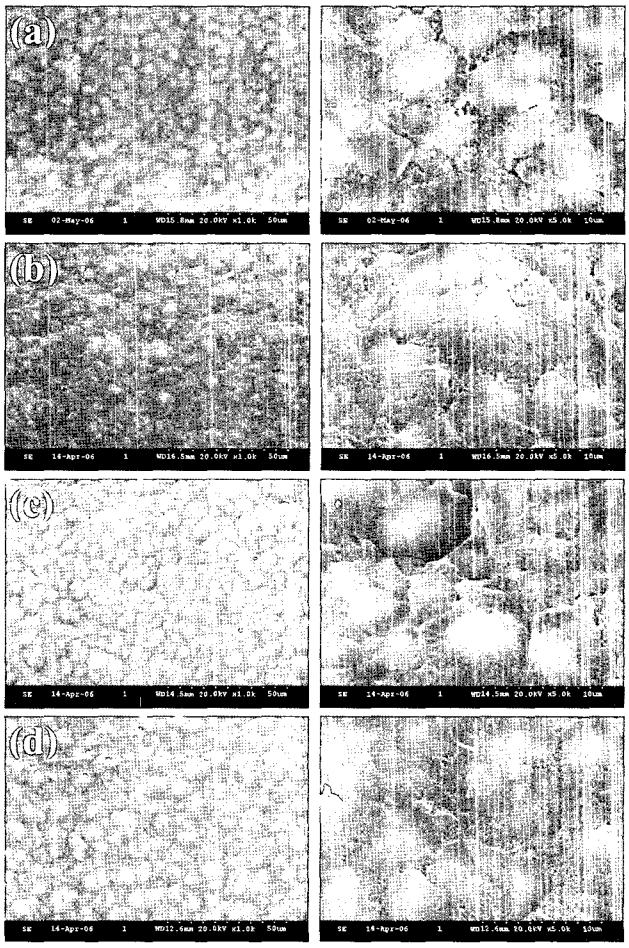


**Figure 1.** Outer (left) and magnified surface (right) SEM photographs of hollow fiber membranes prepared without PVP (a) and with 3 wt% of PVP at molecular weight of (b) 10 k, (c) 55 k, and (d) 900 k.

indicates that the crystallization of PVDF occurs prior to liquid-liquid demixing, as reported previously.[20] Besides, the surface morphology seems to become smooth after addition of PVP, which imply that crystallization of PVP is suppressed by miscibility between PVP and PVDF.

It is important to mention that a good solvent for PVDF such as DMAc was included in the coagulant bath. The addition of a solvent into an immersion precipitation bath lowers polymer concentration at the interfacial region through dissolution. Thus, crystal growth at the interface may be inhibited due to the low interfacial polymer content and fast cooling. Furthermore, low exchange rate of solvent for non-solvent may sufficiently delay liquid-liquid demixing rate and crystallization becomes dominant under such conditions. As a result, a porous structure at the surface is formed with a great number of spherical particles, which confirms that crystallization process with cooling governs the formation mechanism of the membranes.

Figure 2 shows the cross-sectional SEM photographs of hollow fiber membranes. All membranes are nearly symmetric without the formation of noticeable skin layer. In addition, in the same tale with the surface images, all membranes comprise of a number of spherical particles revealing porous paths networked among particles. The formation of a skin layer in the case of amorphous polymers is well understood and is related to the increase of polymer concentration at the outer and inner side of the solution by low mutual diffusion between solvent and non-solvent during the precipitation process.[5] In case of a crystalline polymer such as PVDF, the exchange rate of solvent for non-solvent is slow due to the addition of a good solvent into the coagulation bath. Under such precipitation conditions, the formation of more nuclei and the growth of crystal phases are more favorable than liquid-liquid phase separation. Consequently, crystalline rearrangements grow until the crystallization process is hindered by the increase of crystals in the neighborhood without the formation of a significant skin layer, resulting in a porous structure composed of many crystals.

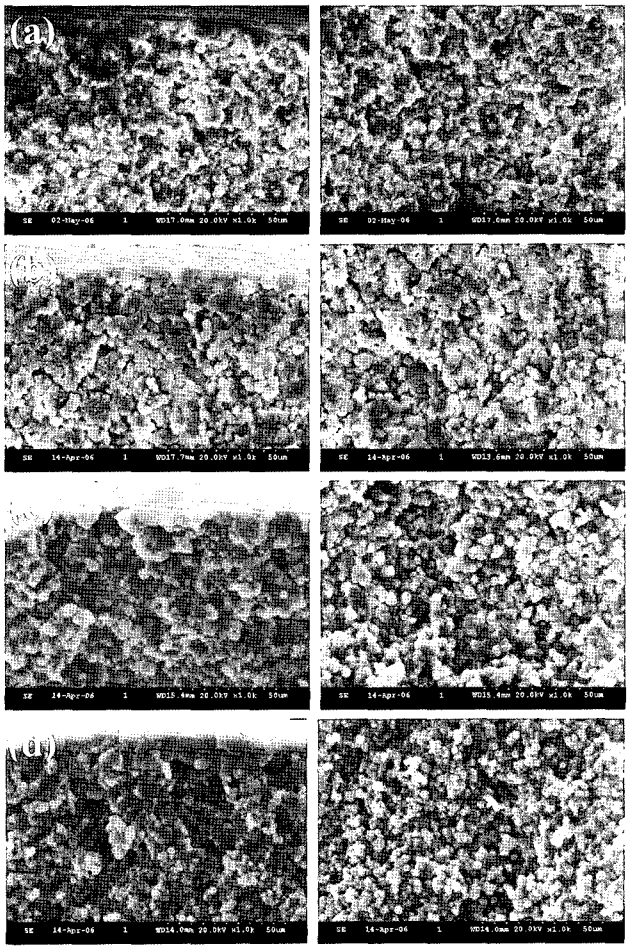

**Figure 2.** Cross-sectional SEM photographs of outer (left) and middle part (right) hollow fiber membranes prepared without PVP (a) and with 3 wt% of PVP at molecular weights of (b) 10 k, (c) 55 k, and (d) 900 k.

It is important to note that the membrane structure without PVP is clearly different from those containing PVP. For example, it was found that the sizes of the spherical particles in Figure 2(a) decreased by adding PVP, as shown in Figure 2(d). This indicates that PVP miscible with PVDF significantly inhibits the degree of crystallization as well as crystallinity of PVDF, resulting in the reduction of size of particles.

**Thermal Properties and Crystal Structures of PVDF Hollow Fibers.** The degree of crystallization and crystallinity of samples as well as their melting points were investigated using DSC and the results are summarized in Table I. The melting peak temperature ($T_m$) and melting enthalpy ($\Delta H_m$) were determined from the DSC curves. The melting point of fiber without PVP was determined at 174.1 °C, which is in good agreement with previous result.[21] It was found that the melting point slightly decreased after the addition of PVP. As well known, the melting point of a crystalline polymer is lowered by the addition of a polymer that is miscible with the amorphous segments of semi-crystalline polymers. Thus, the depression of melting point clearly indicates that an

**Table I. Thermal and Mechanical Properties of PVDF Hollow Fiber Membranes Prepared from Different Molecular Weights of PVP**

| PVP Molecular Weight | $T_m$[a] (°C) | $\Delta H_m$[a] (J g$^{-1}$) | $X_c$ (%) | Elongation Strength (gf/fiber) |
|---|---|---|---|---|
| None | 174.1 | 44.8 | 42.8 | 303.3 ± 5 |
| 10 k | 171.6 | 42.5 | 40.6 | 257.6 ± 18 |
| 55 k | 170.9 | 39.3 | 37.5 | 351.5 ± 4 |
| 900 k | 170.8 | 34.8 | 33.2 | 344.4 ± 6 |

[a]Attained from second scan.

amorphous part of PVDF is miscible with PVP, although the degree of depression in this case was very low because of small amounts of PVP used. Table I also shows a clear decrease of melting enthalpy with adding PVP. Such decrease of fiber properties can be understood in terms of the decrease of crystallinity in the increase of amorphous segments with addition of PVP. The decrease of melting enthalpy is also accompanied with the reduction of crystallinity, as presented in Table I. The overall crystallinity was evaluated by the formula $X_c$ (%) = $\Delta H_m/\Delta H_{100} \times 100$, where $\Delta H_{100}$ is the calculated melting enthalpy, considering the polymer to be 100% crystalline, $\Delta H_{100}$ = 104.7 J g$^{-1}$ for PVDF.[16,22] As expected, crystallinity of hollow fibers decreased from 42.8 to 33.2%, which indicates that the addition of PVP inhibits the degree of crystallization of PVDF, as evidenced by the decrease of crystal size from SEM analysis.

For a better understanding of the change of crystal structure of PVDF hollow fiber membranes by addition of PVP, wide-angle X-ray diffraction (WAXD) study was performed. PVDF is known to crystallize in several different crystal polymorphs such as $\alpha$, $\beta$, $\gamma$ and $\delta$, depending on processing conditions such as solvent, temperature, and polymer concentration used. For instance, the PVDF gel structure in cyclohexane shows $\alpha$-type crystallite having TGTG conformation, whereas it has crystal structure of $\gamma$-form with GTTT conformation in $\gamma$-BL.[18] This difference was mainly ascribed to interactions such as hydrogen bonding between PVDF and $\gamma$-BL. On the other hand, it was reported that $\beta$-type gel structure was overwhelmed by the formation of both $\alpha$- and $\beta$-form crystallites with decreasing PVDF concentration in $\gamma$-BL solvent.[16] The latter with low PVDF concentration corresponds to liquid-liquid phase separation in the early stage of gelation followed by crystallization in the final stage, whereas the former with high PVDF concentration is due mainly to crystallization. In addition, it is known that when PVDF is crystallized at a high or moderate cooling depth such as supercooling or quenching, rapid crystallization yields the more kinetically favored α crystal form.[23]

Figure 3 shows the change of XRD patterns of samples with and without PVP. For the fiber without PVP, there are three main peaks at about $2\theta$= 18.8 and 27.0 together with a strong peak at 20.4, which are consistent with the diffraction positions of neat PVDF containing both $\alpha$- and $\beta$- polymorph crystals, as reported before.[16,18,24] After addition of PVP, the characteristic reflection due to $\alpha$-polymorphic form at $2\theta$=20.4 largely attenuated, leaving only a broad reflection at about 18.8 and 27.0. The result implies that the crystallites of the PVDF membrane as mixture of $\alpha$-and $\beta$-form crystallites rearrange to dominantly $\gamma$-form crystallites, as reported previously.[25]

**Microfiltration Performance and Pore Size of PVDF Hollow Fibers.** For microfiltration performance evaluation, dead-end flow measurements were carried out. Water flux and percent of rejection was measured with pure deionized water and a solution containing polystyrene latex particle (25 ppm) at 1 kg/cm$^2$ feed pressure and ambient condition. Figure 4 shows the change of water flux and rejection rate of hollow fiber membranes measured as a function of PVP molecular weights. It is obvious that water flux slightly decreased, while rejection rate significantly increased after the addition of PVP. Although an increase of water permeability due to the enhancement of hydrophilicity can be easily expected, the introduction of PVP didn't necessarily lead to the increase of water permeability, which can be understood in terms of the reduction of apparent pore size due to the

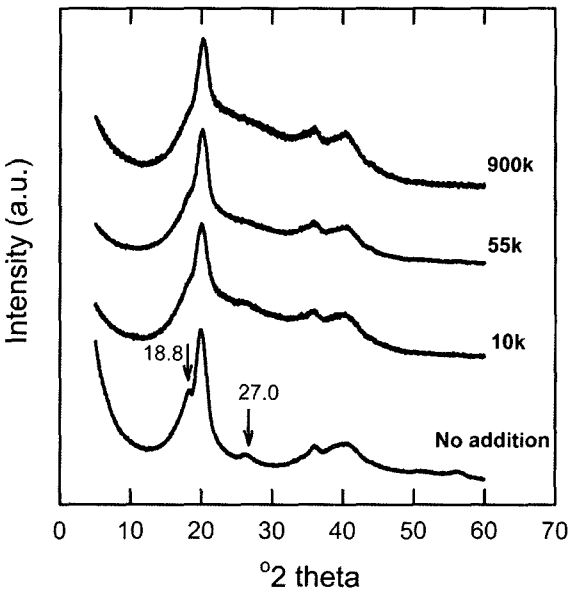


**Figure 3.** The change of WAXD patterns of PVDF hollow fiber membranes with and without PVP.

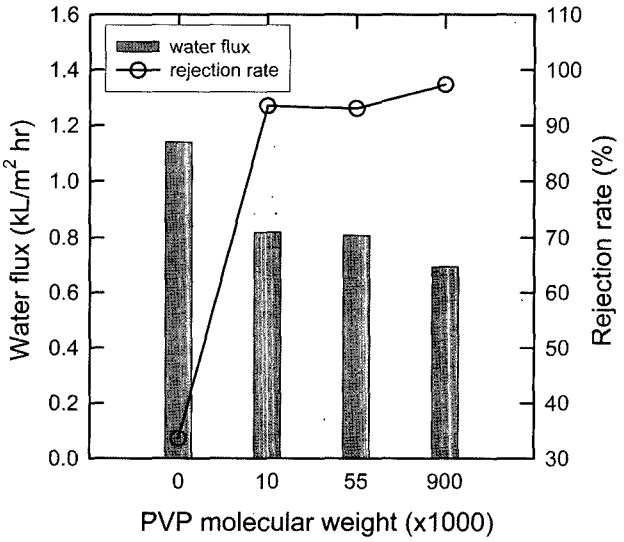


**Figure 4.** The change of water flux and rejection rate as a function of PVP molecular weight.

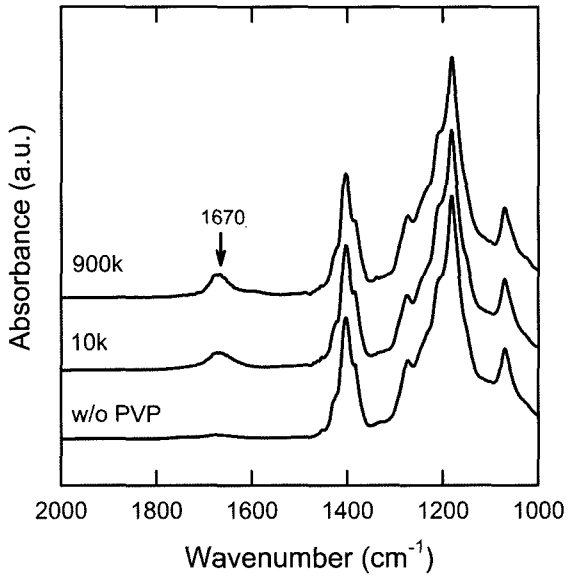


**Figure 5.** ATR-FTIR spectra of PVDF hollow fiber membranes with and without PVP.

swelling of PVP entrapped into pore walls during water permeation, as described previously.[9] To support the retainment of PVP into PVDF matrix, ATR-FTIR measurement was performed and the result was shown in Figure 5. It is obvious that there is no peak corresponding to the carbonyl group of PVP in the range 1600 and 1700 $cm^{-1}$. However, after addition of PVP, a new peak appears at about 1670 $cm^{-1}$, which indicate that PVP was remained into PVDF matrix. Additionally, it is noted that the permeability and permeate rejection in microfiltration process are two competing factors that must be optimized. Thus, it was found that to effectively block the particle or to reach a high rejection ratio (>90.0%) without the accompanying significant loss in water flux, the PVP molecular weight in a spinning solution should be around 10,000. A further increase in the molecular weight would start to decrease the water flux.

To further support the reduction of pore size due to the addition of PVP, capillary flow porometry was used to investigate the pore structure of the hollow fiber membranes with PVP (10 k) and without PVP. The differential pressure at which the wet curve intersects the half-dry curve was used to compute the mean flow pore diameter of the constricted part of the through pores. The mean pore size measured for the fiber with PVP was 0.06±0.03 $\mu$m lower than 0.57± 0.24 $\mu$m of the fiber without PVP, which demonstrates that the addition of PVP lowers the mean pore size of membrane as well as the bulk porosity. Besides, it is noted that the bulk porosity is different from surface porosity. Compared with the SEM micrographs, the through pore sizes measured by flow porometry are much smaller than those of the open pores on the membrane surface. This indicates that most of the through-pores for liquid flow are not cylindrical, but have tortuous structures consisting of quite constricted paths since flow porometry measures the constricted part of the though pore sizes of the bulk membrane.

The elongation strength of hollow fibres was also evaluated using a Universal Tester and the result can be seen in Table I. It is well known that the mechanical properties of porous and crystalline materials are mainly governed by porosity and crystallinity. As expected from the reduction in mean pore size, elongation strength of membranes increased after PVP addition. This result implies that the reduction of crystallinity as well as bulk porosity leads to a decrease in the fragility of the membranes and thus, an increase in physical integrity accompanied with the increase of mechanical properties.[26]

## Conclusions

In summary, PVDF hollow fiber membranes with particulate structure were successfully prepared using high-temperature spinning and their porous structures were further controlled using PVP having various molecular weights for the optimization of microfiltration performance. By introducing PVP into a spinning solution, the microfiltration performances could be controlled, resulting in the increase in rejection rate and elongation strength at the expense of the decrease in mean pore size and water flux. The melting enthalpy was also reduced together with the degree of crystallization, reflected by the change of PVDF crystal structure. This strategy for controlling the porous structure of membranes with particulate morphology could be further manipulated for practical and efficient applications such as in microfiltration and ultrafiltration process.

**Acknowledgements.** This research was supported by a grant ($I^2$ WATERTECH04-1) from $I^2$ WaterTech of Eco-STAR project funded by Ministry of Environment, Korea.

## References

(1) P. Witte, P. J. Dijkstra, J. W. A. Berg, and J. Feijen, *J. Membrane Sci.*, **117**, 1 (1996).
(2) D. -J. Lin, K. Beltsios, T. -H. Young, Y. -S. Jeng, and L. -P. Cheng, *J. Membrane Sci.*, **274**, 64 (2006).
(3) L. -P. Cheng, T. -H. Young, L. Fang, and J. -J. Gau, *Polymer*, **40**, 2394 (1999).
(4) X. Tan, S. P. Tan, W. K. Teo, and K. Li, *J. Membrane Sci.*, **271**, 153 (1998).
(5) M. Mulder, *Basic Principles of Membrane Technology*, Kluwer Academic, Dordrecht, The Netherlands, 1992.
(6) L. Y. Lafreniere, F. D. F. Talbot, T. Matsuura, and S. Sourirajan, *Ind. Eng. Chem. Res.*, **26**, 2385 (1987).
(7) M.-C. Yang and T. -Y. Liu, *J. Membrane Sci.*, **226**, 119 (2003).
(8) C. Hying and E. Staude, *J. Membrane Sci.*, **144**, 251 (1998).
(9) J. -J. Qin, F. -S. Wong, Y. Li, and Y. -T. Liu, *J. Membrane*

*Sci.*, **211**, 139 (2003).
(10) J. H. Kim, J. E. You, and C. K. Kim, *Macromol. Res.*, **10**, 209 (2002).
(11) D. Wang, K. Li, and W. K. Teo, *J. Membrane Sci.*, **163**, 211 (1999).
(12) B. J. Cha, K. Char, J. -J. Kim, S. S. Kim, and C. K. Kim, *J. Membrane Sci.*, **108**, 219 (1995).
(13) H. Matsuyama, H. Okafuji, T. Maki, M. Teramoto, and N. Kubota, *J. Membrane Sci.*, **223**, 119 (2003).
(14) B. T. Kim, K. Song, and S. S. Kim, *Macromol. Res.*, **10**, 127 (2002).
(15) K. Tan and S. K. Obendorf, *J. Membrane Sci.*, **274**, 150 (2006).
(16) J. W. Cho, H. Y. Song, and S. Y. Kim, *Polymer*, **34**, 1024 (1993).
(17) B. S. Kim, S. T. Baek, K. W. Song, I. H. Park, J. O. Lee, and N. Nemoto, *J. Macromol. Sci.*, **B43**, 741 (2004).
(18) M. Tazaki, R. Wada, M. Okabe, and T. Homma, *J. Appl. Polym. Sci.*, **65**, 1517 (1997).
(19) B. J. Cha, J. M. Yang, Y. J. Choi, and H. Kim, *J. Membrane Sci.*, submitted.
(20) L.-P. Cheng, *Macromolecules*, **32**, 6668 (1999).
(21) Z. H. Liu, Ph. Marechal, and R. Jerome, *Polymer*, **37**, 5317 (1996).
(22) S. Hietala, S. Holmberg, M. Karjalainen, J. Nsman, M. Paronen, P. Serima, F. Sundhole, and S. Vahvaselk, *J. Mater. Chem.*, **7**, 721 (1997).
(23) B.-E. E. Mohajir and N. Heymans, *Polymer*, **42**, 5661 (2001).
(24) F. A. Landis and R. B. Moore, *Macromolecules*, **33**, 6031 (2000).
(25) N. Chen and L. Hong, *Polymer*, **43**, 1429 (2002).
(26) M. A. Sabino, S. Gonzalez, L. Maequez, and J. L. Feijoo, *Polym. Degrad. Stabil.*, **69**, 209 (2000).